THE JOURNAL OF BIOLOGICAL CHEMISTRY VOL. 287, NO. 13, pp. 10613–10622, March 23, 2012

Three-dimensional Structure of Steroid 21-Hydroxylase (Cytochrome P450 21A2) with Two Substrates Reveals Locations of Disease-associated Variants*[S]

Received for publication, November 13, 2011, and in revised form, December 19, 2011 Published, JBC Papers in Press, January 18, 2012, DOI 10.1074/jbc.M111.323501

Bin Zhao[‡1], **Li Lei**[‡], **Norio Kagawa**[§], **Munirathinam Sundaramoorthy**[‡], **Surajit Banerjee**[‡], **Leslie D. Nagy**[‡], **F. Peter Guengerich**[‡], **and Michael R. Waterman**[‡2]

From the [‡]*Department of Biochemistry and Center in Molecular Toxicology, Vanderbilt University School of Medicine, Nashville, Tennessee 37232-0146 and the* [§]*Global Centers of Excellence Program, Nagoya University Graduate School of Medicine, Nagoya 466-8550, Japan*

Background: Steroid 21-hydroxylase deficiency accounts for ~95% of individuals with congenital adrenal hyperplasia (CAH).
Results: The bovine cytochrome P450 21A2 (CYP21A2) crystal structure complexed with the substrate 17-hydroxyprogesterone was determined to 3.0 Å resolution.
Conclusion: The structure reveals the binding mode of two molecules of the steroid substrate and accurate residue locations in the protein.
Significance: The structure of CYP21A2 enhances our understanding of CAH.

Steroid 21-hydroxylase (cytochrome P450 21A2, CYP21A2) deficiency accounts for ~95% of individuals with congenital adrenal hyperplasia, a common autosomal recessive metabolic disorder of adrenal steroidogenesis. The effects of amino acid mutations on CYP21A2 activity lead to impairment of the synthesis of cortisol and aldosterone and the excessive production of androgens. In order to understand the structural and molecular basis of this group of diseases, the bovine CYP21A2 crystal structure complexed with the substrate 17-hydroxyprogesterone (17OHP) was determined to 3.0 Å resolution. An intriguing result from this structure is that there are two molecules of 17OHP bound to the enzyme, the distal one being located at the entrance of the substrate access channel and the proximal one bound in the active site. The substrate binding features locate the key substrate recognition residues not only around the heme but also along the substrate access channel. In addition, orientation of the skeleton of the proximal molecule is toward the interior of the enzyme away from the substrate access channel. The 17OHP complex of CYP21A2 provides a good relationship between the crystal structure, clinical data, and genetic mutants documented in the literature, thereby enhancing our understanding of congenital adrenal hyperplasia. In addition, the location of certain CYP21A2 mutations provides general understanding of structure/function relationships in P450s.

Cytochrome P450 (P450)[3] 21-hydroxylase (CYP21A2) converts progesterone and 17-hydroxyprogesterone (17OHP) to 11-deoxycorticosterone and 11-deoxycortisol, respectively (Fig. 1) (1, 2). CYP21A2 is expressed in the adrenal cortex and plays an essential role in the biosynthesis of aldosterone and cortisol. Deficiency of CYP21A2 enzymatic activity is the most common cause of congenital adrenal hyperplasia (CAH), an inherited disorder of steroidogenesis (3, 4). There are six CYP proteins (CYP11A1, CYP11B1, CYP11B2, CYP17A1, CYP19A1, and CYP21A2) associated with the synthesis of the steroid hormones in humans. CYP11A1, CYP11B1, and CYP11B2 are located in the inner mitochondrial membrane, and the other CYP proteins, including CYP21A2, are microsomal monooxygenases.

CAH results from complete or partial loss of activity in one of several steroidogenic enzymes. Up to 95% of all cases of CAH are due to CYP21A2 deficiency, which reduces production of cortisol and aldosterone and may lead to excess production of andrenal androgens (3). CAH traditionally has three forms based on clinical phenotypes: a severe form with a concurrent defect in aldosterone biosynthesis (salt-wasting type) and a form with apparently normal aldosterone biosynthesis (simple virilizing type) together termed classic 21-hydroxylase deficiency. There is also a mild, non-classic form that may be asymptomatic or associated with signs of postnatal androgen excess. The worldwide incidence of CAH is 1:15,000 for the classical form and ~1:1,000 for the nonclassic form (3). In humans, there are two *CYP21* genes located in the leukocyte

* This work was supported, in whole or in part, by National Institutes of Health Grants GM69970 (to M. R. W. and F. P. G.), R37 CA090426 (to F. P. G.), and P30 ES000267 (to F. P. G. and M. R. W.).
[S] This article contains supplemental Figs. S1–S3.
The atomic coordinates and structure factors (code 3QZ1) have been deposited in the Protein Data Bank, Research Collaboratory for Structural Bioinformatics, Rutgers University, New Brunswick, NJ (http://www.rcsb.org/).
[1] To whom correspondence may be addressed: Dept. of Biochemistry and Center in Molecular Toxicology, Vanderbilt University School of Medicine, 632 Robinson Research Bldg., 2200 Pierce Ave., Nashville, TN 37232-0146. Tel.: 615-343-4644; Fax: 615-343-0704; E-mail: bin.zhao@vanderbilt.edu.
[2] To whom correspondence may be addressed: Dept. of Biochemistry and Center in Molecular Toxicology, Vanderbilt University School of Medicine, 632 Robinson Research Bldg., 2200 Pierce Ave., Nashville, TN 37232-0146. Tel.: 615-343-4644; Fax: 615-343-0704; E-mail: Michael.Waterman@vanderbilt.edu.

[3] The abbreviations used are: P450, cytochrome P450; CAH, congenital adrenal hyperplasia; 17OHP, 17-hydroxyprogesterone; C3B21RA, C3B21T241R/L442A.

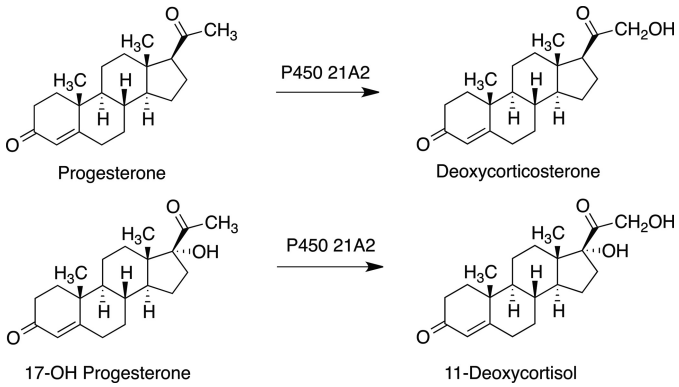

FIGURE 1. **Reactions catalyzed by CYP21A2.**

antigen class III locus in chromosome 6 (band 6p21.3): a pseudogene, *CYP21A1*, and the functional *CYP21A2*. Recombination of the *CYP21A2* gene with *CYP21A1* leads to gene deletion or insertion mutations of CYP21A2, one reason for alteration of 21-hydroxylase activity being the primary cause of CAH (5–7). In addition, rare point mutations that arise independently of the pseudogene have been recorded to date, due to the location of *CYP21A2* in a locus in chromosome 6, where mutations are not uncommon among the resulting proteins (for details, see the Human Gene Mutation Database Web site). A total of >150 CYP21A2 mutations are currently reported, of which at least 97 are the missense type. Although CYP21A2 has been the subject of biochemical studies for the past several decades by clinical evaluation of patients and/or by measuring enzyme activities of recombinant proteins in cultured cells (8) and by structural prediction using different homology models (9, 10) based on other known P450 structures, many aspects of CYP21A2 biochemistry and especially the structural basis of the mutants causing CAH remain poorly understood (11–14).

Here we report the crystal structure of bovine CYP21A2 complexed with 17OHP. The crystal structure reveals the binding mode of two molecules of the steroid substrate and accurate residue locations on the protein. Also it indicates the specific interactions between different secondary structural elements through hydrogen bonding networks that play important roles on local and/or overall CYP21A2 structural folding (supplemental Fig. S1). This detailed structural information from CYP21A2 enhances our understanding of the molecular basis of CAH and also provides insight into P450 structure/function relationships in general.

EXPERIMENTAL PROCEDURES

Expression and Purification of Engineered CYP21A2 (C3B21RA)—In order to obtain a soluble form of bovine CYP21A2 for crystallization experiments, two surface residues were mutated, Thr-241 (to Arg) and Leu-442 (to Ala). The synthetic oligonucleotides used for site-directed mutagenesis were as follows: C3B21T241R forward primer (5′-gaagcagctgCGGcgccacagg) and the reverse primer (5′-cctgtggcgCCGcagctgcttc). The C3B21T241R/L442A forward primer was 5′-cgtggtgctcGCGcgactgctgcag, and the reverse primer was 5′-ctgcagcagtcgCGCgagcaccacg. C3B21 was used as template to obtain C3B21T241R, which was then used as the template for C3B21T241R/L442A (C3B21RA). The changes were confirmed by nucleotide sequence analysis (the PCR is described in Ref. 15). The reaction was carried out using the following cycling parameters: 95 °C for 30 s, 55 °C for 1 min, 68 °C for 7 min for 25 cycles and 68 °C for 6 min. Then 40 μl of the reaction (to which 1 μl of the restriction enzyme DpnI had been added) was incubated at 37 °C for 2 h, after which 2 μl of the DpnI-treated reaction was transformed into 50 μl of *Escherichia coli* DH5α cells. Following culture at 37 °C for 1 h, the cells were spread on an agar plate containing 100 μg/ml ampicillin.

The C3B21RA protein was expressed and purified as reported earlier (16). In brief, cells co-transformed with the plasmids CYP21A2pET17b and pGro12 were cultured overnight in LB broth containing 100 μg/ml ampicillin and 50 μg/ml kanamycin. After inoculation (1:100, v/v) in 3 liters of Terrific Broth containing 100 μg/ml ampicillin and 50 μg/ml kanamycin, growth was carried out at 37 °C and 240 rpm for 6 h. Then 1 mM isopropyl 1-thio-β-D-galactopyranoside, 1 mM δ-aminolevulinic acid, and 4 mg/ml arabinose were added, and culture was incubated for another 38 h at 27 °C. Cells were harvested by centrifugation (2850 × *g*, 20 min at 4 °C) and resuspended in 100 ml of TES buffer (250 mM sucrose, 50 mM Tris-HCl (pH 7.4), 0.5 mM EDTA) containing 1 mg/ml lysozyme. After incubation on ice for 30 min, the sample was centrifuged again. Cell pellets were sonicated in 250 ml of buffer A (50 mM potassium phosphate (pH 7.4), containing 20% glycerol (v/v), 0.1 mM dithiothreitol, 0.1 mM EDTA, 300 mM sodium chloride, 1.5% sodium cholate (w/v), 1% Tween 20 (w/v), and 0.1 mM phenylmethylsulfonyl fluoride). The supernatant (250 ml, 1200 nmol of CYP21A2) was applied on a nickel-NTA-agarose column (3 cm × 3 cm) equilibrated with buffer A. The column was washed with buffer A containing 20 mM imidazole, followed by buffer B (20 mM potassium phosphate (pH 7.4) containing 20% glycerol (v/v), 0.1 mM dithiothreitol, 0.1 mM EDTA, 1.0% sodium cholate (w/v), 1% Tween 20 (w/v), and 100 μM phenylmethylsulfonyl fluoride) and eluted with buffer C (50 mM potassium phosphate (pH 7.4) containing 20% glycerol (v/v), 0.1 mM dithiothreitol, 0.1 mM EDTA, and 1% sodium cholate, w/v) containing 100 mM imidazole. The eluate was applied to a DEAE-Sepharose column (2 cm × 9 cm) and washed with 20 mM potassium phosphate buffer (pH 7.4) containing 20% glycerol (v/v), 0.1 mM dithiothreitol, 0.1 mM EDTA, and 1.0% sodium cholate (w/v). The flow-through fraction was applied to an SP-Sepharose column (2 cm × 6 cm) and washed with buffer D (50 mM potassium phosphate, pH 7.4, 20% glycerol, 0.1 mM DTT, 0.1 mM EDTA, 0.25% Cymal 5, and 50 mM NaCl, and the engineered form of CYP21A2 was eluted with a linear 50–300 mM NaCl gradient in the same buffer.

Catalytic Activity Assay—The procedure was modified from previous work (16). Preliminary experiments showed very similar rates of progesterone 21-hydroxylation by both a truncated P450 21A2 (16) and the C3B21RA mutant in 0.002% (w/v) Cymal 5 detergent and with 30 μM L-α-dilauroyl-*sn*-glycero-3-phosphocholine vesicles, a commonly used P450 reconstitution system. For the determination of steady-state kinetic parameters, incubations contained 2 pmol of P450 21A2 (either the truncated version (16) or the C3B21RA mutant), 60 pmol of *E. coli* recombinant NADPH-P450 reductase (17, 18), 2 μg of L-α-dilauroyl-*sn*-glycero-3-phosphocholine, and varying con-

centrations of [4-^{14}C]progesterone (51 mCi/mmol; American Radiolabeled Chemicals (St. Louis, MO); Lot 030610, 0.3–20 μM) in 85 μl of 50 mM potassium phosphate buffer. Preincubation was at 37 °C for 5 min, and reactions were initiated by the addition of 15 μl of an NADPH-generating system (final concentrations (in reaction) of 10 mM glucose 6-phosphate, 1 mM $NADP^+$, and 2 μg ml^{-1} yeast glucose 6-phosphate dehydrogenase). After reaction for 2 min at 37 °C, reactions were quenched by the addition of 50 μl of CH_3OH and chilled on ice.

A 50-μl aliquot of each reaction was spotted directly to the loading zone of a Whatman LK5DF silica gel TLC plate (20 cm × 20 cm). Authentic (unlabeled) standards of progesterone and 11-deoxycorticosterone were added to some of the lanes. The plates were dried in air in a fume hood (with the door open 15 cm to generate a draft), and the plates were developed in CH_2Cl_2/ethyl acetate (4:1, v/v), dried in the same way as described above, and visualized under 254-nm UV light. The zones containing 11-deoxycorticosterone and progesterone were removed by scraping (from individual lanes), and 1.0 ml of CH_3OH was added to each (to extract the steroids), followed by 5.0 ml of ScintiVerse II liquid scintillation mixture (Fisher). Radioactivity was quantified using a Beckman LS6500 scintillation counter, and recovery was based upon [^{14}C]progesterone samples eluted from the same plates.

The parameters k_{cat} and K_m were derived from plots of reaction velocity *versus* substrate concentration fit to hyperbolae using non-linear regression analysis (GraphPad Prism 5.0c, GraphPad, San Diego, CA).

Spectral Analyses of CYP21A2—Steady-state binding experiments were made using UV-visible spectroscopy using an Aminco 2Wa-OLIS spectrophotometer (On-Line Instrument Co., Bogart, GA). Both cuvettes (1.0-ml) contained 2.0 μM P450 21A2 in 50 mM potassium phosphate buffer. Aliquots (0.5 μl) of 400 μM progesterone or 21-hydroxyprogesterone (in C_2H_5OH) were added to the sample cuvette, with an equivalent amount of ethanol added to the reference cuvette. Spectra (350–500 nm) were recorded at 23 °C. Data points were fit to a two-site model, with correction for enzyme depletion, using the program DynaFit (supplemental Fig. S2).

Pre-steady-state binding kinetics were recorded at 37 °C with an OLIS RSM-1000 stopped-flow spectrophotometer, operating in the full scanning mode (collecting spectra from 310 to 530 nm). One syringe contained 4.0 μM P450 21A2 in 50 mM potassium phosphate buffer (pH 7.4) containing 100 mM NaCl, 0.1 mM dithiothreitol, and 0.1 mM EDTA. The other syringe contained 40 μM progesterone or 17-hydroxyprogesterone in the same buffer. Spectral (scanning) data were collected for 20 s, and the kinetic traces at 390 and 418 nm (20-nm scan width, single variable decomposition) were fit to biexponential equations using the manufacturer's software.

Crystallization, Data Collection, and Structure Determination—0.2 mM CYP21A2 (C3B21RA) in buffer D was co-crystallized with 17OHP (0.4 mM, containing 2% (v/v) C_2H_5OH) grown by the hanging drop vapor diffusion method using 5–15% (w/v) polyethylene glycol 3350, 0.5 M ammonium sulfate, and 0.1 M HEPES (pH 7.0) as the mother liquor. At 20 °C, the ferric 17OHP-bound crystals appeared within a few days. Cryoprotection was achieved by soaking the crystals in 30% (v/v) ethylene glycol prior to flash freezing in liquid nitrogen.

All diffraction data were collected at 100 K at the Southeast Regional Collaborative Access Team (SER-CAT) 21-ID beamline and the Life Science Collaborative Access Team (LS-CAT) beamline, both at the Advanced Photon Source, Argonne National Laboratory. The x-ray data were processed and scaled with the HKL package programs HKL2000 (19). The crystals belong to the monoclinic space group $P2_1$ with the following unit cell parameters: $a = 67.87$ Å, $b = 167.99$ Å, $c = 111.84$ Å, $\beta = 90.08°$. The resolution is 3.38 Å with a 2.0 $I/\sigma I$ cut-off, which is extended to 3 Å due to the completeness over 90% in the highest resolution shell. The structure was determined by molecular replacement using the program PHASER (20) and the rabbit CYP2C5 structure as a search model because CYP2C5 has progesterone 21-hydroxylase activity and 30% sequence identity to bovine CYP21A2. The initial model was built in COOT (21), and refinement was performed using CNS1.3 (22) in space group $P2_12_12$, and CNS parameter and topology files were generated by PRODRG (23). There were two molecules of CYP21A2 in the asymmetric unit. However, the refinement did not progress well in space group $P2_12_12$, the *R*-free did not improve substantially beyond 38% at 3.0 Å resolution, and the Ramachandran plot diverged during the refinement. The analysis of intensity statistics using CNS1.3 (22) and twinning server (24) revealed that the data sets are affected by perfect hemihedral twinning. The proper space group for CYP21A2 crystals is $P2_1$ rather than $P2_12_12$. The twinning is probably coupled with non-crystallographic symmetry in the $P2_1$ space group and indicates there are four CYP21A2 molecules in the asymmetric unit. The data were reprocessed in the $P2_1$ space group, and refinement was performed against intensities using the protocols for twinned data (twinning operator $-h,k,-l$), a fixed twin fraction of 0.5. The *R*-free dropped to 33% after the rigid body refinement in the $P2_1$ space group at 3.0 Å resolution. After several rounds of positional, *B*-factor, and slow annealing refinements alternated with manual model building, the water molecules were added automatically in CNS. Finally, the non-crystallographic symmetry restraint was removed, and with several rounds of refinement, the *R* values were reduced to 28.3% (*R*-work) and 29.6% (*R*-free) at 3.0 Å. Final refinement statistics are given in Table 1. All structural figures were prepared with the program PyMOL (25).

RESULTS

Substrate Binding and Catalytic Activity of CYP21A2—Wild-type bovine CYP21A2 has been efficiently expressed in *E. coli* (16). At lower concentrations, the protein showed the expected catalytic activity, which suggests that the protein is stable and properly folded. However, the poor solubility of the protein disrupted attempts at crystallization. To enhance the protein solubility (26), we engineered hydrophobic residues exposed to solvent, based on multiple mammalian CYP21A2 sequences, including human and bovine (supplemental Fig. S1). The greatly improved solubility properties of the mutant containing the T241R and L442A substitutions led to successful crystallization. In order to test whether C3B21RA has the same functional activity as the wild-type protein, both titration and enzy-

TABLE 1
Data collection and refinement of CYP21A2 (C3B21RA) structure (17OHP-bound CYP21A2 complex)

Data collection statistics	
Space group	$P2_1$
Unit cell constants	$a = 67.87$ Å, $b = 167.99$ Å, $c = 111.84$ Å $\beta = 90.08°$
Wavelength (Å)	0.97
Total observations	183,838
Unique reflections	47,485
Completeness (%)	95.1 (91.9)[a]
$I/\sigma(I)$	4.5 (1.2)
R_{merge} (%)	9.2 (53.9)
Refinement statistics	
Resolution range (Å)	30–3.0
No. of reflections used in refinement	47,168
No. of water molecules	100
Protein atoms[b]	14,144
Heme atoms	172[c]
Ligand atoms	112[d]
R_{work}/R_{free} (%)	28.3/29.6
Root mean square deviation, bond lengths (Å)	0.01
Root mean square deviation, bond angles (degrees)	1.63

[a] Values for the highest resolution shell are shown in parentheses.
[b] Residues 29–130/133–268/274–409/413–483 (A), 29–130/135–263/274–326/332–483 (B), 29–130/133–263/274–326/332–482 (C), 29–130/134–263/274–326/333–481 (D).
[c] Four heme molecules.
[d] Eight 17OHP molecules.

matic activities were measured. For substrate binding, both biological substrates, progesterone and 17OHP, produced a typical type I P450 binding spectrum in which the Soret band shifted from 418 to 390 nm upon binding, indicating that progesterone and 17OHP can access the heme in the active site. The k_{cat} and K_m values determined for the C3B21RA mutant were 13 ± 2 min^{-1} and 2.4 ± 0.9 μM, respectively. These values are slightly lower than the corresponding values measured for the truncated wild-type protein (24 ± 3 min^{-1}, 1.7 ± 0.7 μM), previous measurements with the unmutated protein (k_{cat} 13 ± 6 min^{-1}, K_m 1.9 ± 0.9 μM), and earlier preparations isolated from bovine adrenals (16).

Overall Structure of Bovine CYP21A2—In order to understand the structural relationship with CAH, an engineered CYP21A2 (C3B21RA) structure complex with 17OHP was determined at a maximum resolution of 3.0 Å. The overall structure of the engineered CYP21A2 exhibits the typical P450 fold consisting of α-helical and β sheet domains as seen in all other known P450 structures (Fig. 2). In detail, the tertiary structure consists of 12 major α-helices, which are similar to those found in most other P450s. However, there are only two groups of sheets with six β-strands in the structure instead of four groups of sheets with 10 β-strands as in most of the other P450s (27, 28). The β sheets in CYP21A2 only include a mixed four-stranded sheet 1 (β1, 58–62; β2, 69–73, β3, 364–366; and β4, 381–386) close to the N-terminal region and two anti-parallel strands in sheet 2 (β5, 451–453; β6, 476–478) at the C terminus. This feature indicates that there are more loop structural elements in CYP21A2 than in many of the other P450 structures. For example, the loop structural residues in CYP21A2 are about 52% in total structural residues compared with 45% loop residues in the CYP11A1 structure (29). The other interesting feature is a kink present in each of the B, E, and J helices. One example is the hydrogen bond between the side chain of Lys-75 in the N terminus of the B helix and the hydroxyl of Ser-416 in the meander region (30). Another hydrogen bond between the side chain of Glu-80 in the C terminus of the B helix and the carbonyl of Ser-371 in a β loop (β3 and β4)

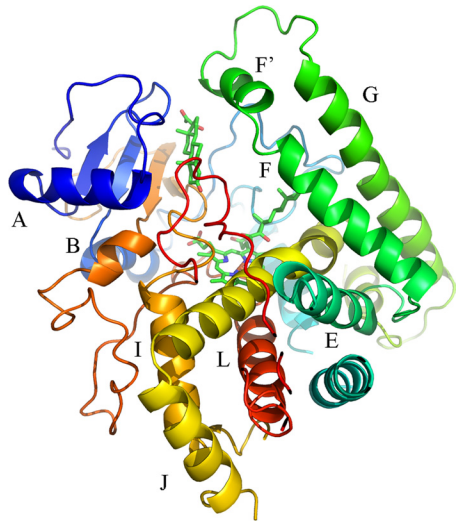

FIGURE 2. ***Ribbon diagram* of the 17OHP-bound engineered CYP21A2 (C3B21RA) structure.** The heme and the two 17OHP molecules are *colored green* in *stick models*. The F helix is stretched into two short helices, and the F′/G helices swing away from the structural core.

together cause stretching, which breaks the B helix into two pieces. These hydrogen bonds also connect the meander region and β sheet 1 through the B helix. Another example is that three residues (Thr-160, Gln-162, and Glu-164) located in the N terminus of the E helix form hydrogen bonds with Gln-477 in β 6, His-190 in the F helix, and Ser-300 in the I helix, resulting in a kink in the E helix. In addition, there is a break in the J helix. The side chains of Arg-315 and Gln-317 in the N terminus of the J helix engage in hydrogen bonds with the side chains of Asp-406 in the meander region and Gln-477 in β6. The side chain of Asp-321 in the C terminus of the J helix hydrogen bonds with the side chain of Arg-483 in β6. Thus, these interactions between the meander region, the J helix, and β6 maintain the secondary structural elements in the correct positions to keep the proper local folding of the CYP21A2. Also, the J helix is stretched into two shorter helices to meet the overall structural requirements. Arg-483 and Gln-481 can launch an extensive

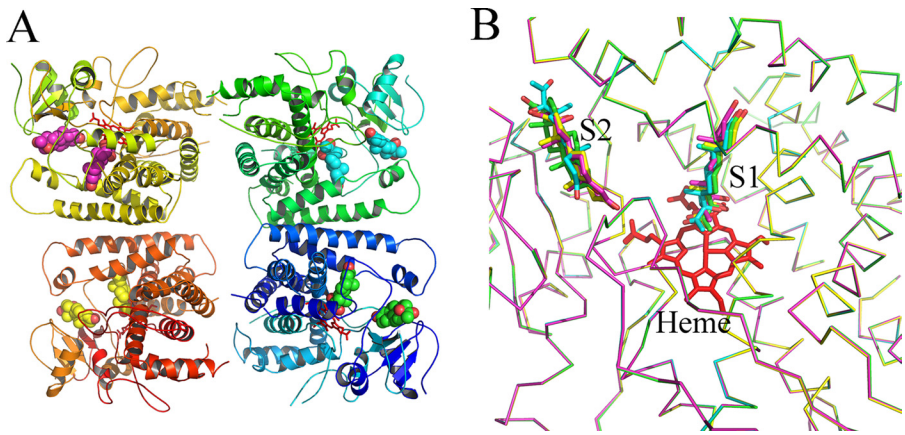

FIGURE 3. **Evidence for the presence of four molecules present in the asymmetric unit cell.** *A*, the four CYP21A2 structures are *colored* in *green*, *yellow*, *blue*, and *orange*. The two molecules of 17OHP are seen in *cyan*, *pink*, *green*, and *yellow* as a *sphere model*. Heme is in a *red stick model*. *B*, superimposed overall structures of 17OHP-bound CYP21A2 as a *backbone stick model*. All four proximal 17OHP molecules are in the same orientation, and the locations of the four distal 17OHP molecules show small variations in binding modes in the substrate access channel.

hydrogen-bonding network in the region of the C terminus and extend the network to the J helix and the meander region, which may stabilize the local structure, including the C terminus and the meander region.

Another feature in the secondary structure of CYP21A2 is that the F helix is twisted into two different helices, which are observed in only a few other P450s (*e.g.* human CYP51 (31)) although the F′ helix in CYP51 is not associated with the ligand. The F′ helix with the F′G loop swings away from the axis of the F helix and is bent toward the B′ helix. As discussed below, this region of the structure contributes significantly to substrate binding. In addition, the N-terminal residues 29–33 form close contacts with residues 373–376, which are located on a β-hairpin loop between β3 and β4. Although there are no hydrogen bonds among these residues, the distance between the backbone amide nitrogen of Leu-30 and the side chain of Tyr-375 is 3.5 Å, and the distance between the carbon of Pro-31 and the side chain of Tyr-375 is 2.9 Å, which conserves close contacts between the N-terminal loop and the β-hairpin loop (β3 and β4). In general, the secondary structural elements in the engineered CYP21A2 are well defined among loops, sheets, and helices. They stabilize each other through hydrogen bonding networks and van der Waals interactions. In addition, mutant T241R is located on the C-terminal end of the G helix, and the side chain of the arginine substitution is exposed to solvent. L442A is at the end of the L helix, and there is space left for the leucine. Thus, the original amino acids from the wild type would not be expected to affect the structure of the engineered protein.

Active Site Cavity—The most striking feature of the tertiary CYP21A2 structure is that there are two molecules of 17OHP present in the active site of each of the four CYP21A2 structures per crystallographic asymmetric unit (Fig. 3*A*). The electron density maps in the region of the active site clearly reveal two bound substrate molecules (Fig. 4). The overall shape of the electron densities agrees with the structure of substrate added in the co-crystallization experiments. One 17OHP ligand is situated in the proximal portion of the CYP21A2 active site over the heme; the other 17OHP is bound at the substrate entrance located between loops β1/β2 and β3/β4 and the F′ helix in a

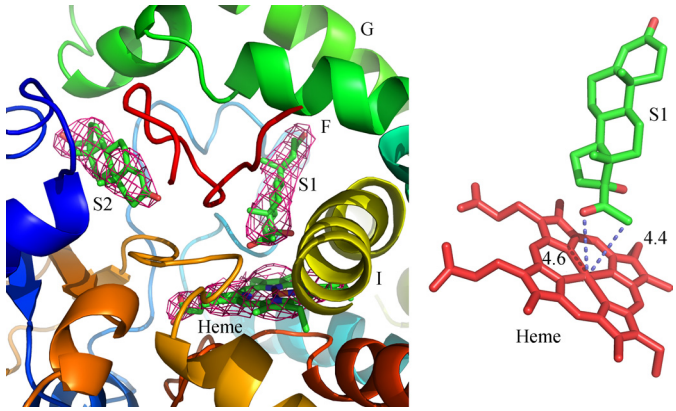

FIGURE 4. **Electron density for 17OHP in the structure of 17OHP-bound CYP21A2.** The electron density map was calculated using σA-weighted $2|F_o| - |F_c|$ coefficients and is contoured at 1.0 σ. The proximal 17OHP and distal 17OHP molecules in the *green stick models* (*left*) are denoted *S1* and *S2*, respectively. Potential hydrogen bonds and the distances between the corresponding carbon and oxygen atoms to the iron atom are shown as *dotted lines* (*right*).

cleft on the distal surface of the protein. This distal 17OHP is partially exposed to the bulk solvent and is ~10 Å away from the proximal substrate molecule. The superimposition of the four molecules (Fig. 3*B*) indicates that all four proximal 17OHPs are in the same orientation and that the substrates are stable in the active site of the enzyme. The four distal 17OHP molecules show a small variation in the binding modes in the substrate access channel because the corresponding secondary structures, such as β1/β2 and β3/β4 loops and F′ helices, are located in slightly different positions. This may suggest that substrate entry structural elements are more dynamic and that the distal substrates may be in different binding stages. The two bound molecules in one enzyme clearly define the substrate access path from the protein surface into the buried active site (Fig. 5). The proximal 17OHP lies over the heme plane and forms an angle of about 45°, thereby tilting toward the G helix. The 3-keto oxygen of the A-ring in the proximal 17OHP establishes a hydrogen bond (2.4 Å) with the guanidinium group of the Arg-232 side chain, located in the middle of the G helix. Thus, the substrate is anchored by the G helix at the A-ring, thereby positioning the carbon of the C21 methyl group over

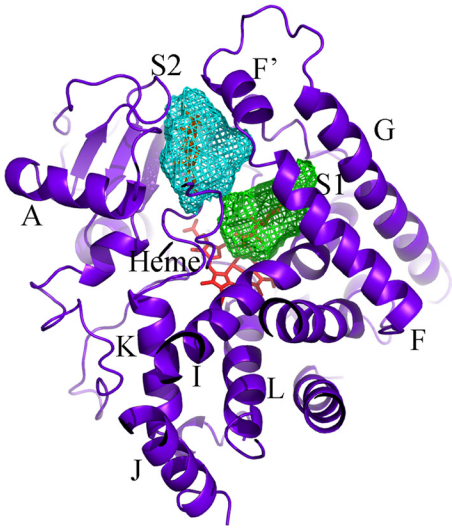

FIGURE 5. **Solvent-accessible surfaces of the substrate binding cavities of CYP21A2.** The cavities are shown as *mesh surfaces*. The distal binding site in the substrate access channel is in *cyan*, and the proximal binding site in the heme pocket is *green*. These two binding sites are connected by a narrow channel.

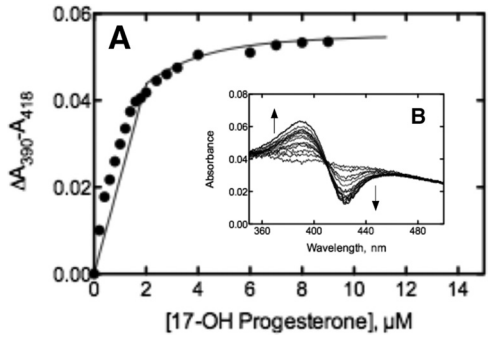

FIGURE 6. **Steady-state binding of 17OHP to CYP21A2.** Two 1.0-ml cuvettes each contained 2.0 μM P450 21A2 in 50 mM potassium phosphate buffer (pH 7.4). A base line was recorded (OLIS-Amico DW2a spectrophotometer), and 1-μl aliquots of 400 μM 17OHP (in C_2H_5OH) were added to the sample cuvette, with an equivalent amount of C_2H_5OH added to the reference cuvette at each step (*B*, *inset*). The points ($\Delta A_{390} - A_{418}$) were fit (using the program DynaFit) to a two-site model with $K_{d,1} = 0.05$ μM, $K_{d,2} = 0.7$ μM (*A*) (using $\Delta\epsilon_1 = \Delta\epsilon_2 = 26$ mM^{-1} cm^{-1}) (supplemental Fig. S1). See Fig. 7 for pre-steady-state data of spectral changes.

the heme iron at a distance of 4.4 Å. Furthermore, the 20-keto oxygen of the substrate is situated at a distance of 4.6 Å from the heme iron, which may allow a hydrogen bonding interaction with the oxygen atom to help binding or proton transfer and dioxygen scission during the CYP21A2 catalytic reaction cycle (32, 33). Thus, the 20-keto group might be part of a pharmacophore of the substrates for their biological activities.

Surprisingly, the distal 17OHP in CYP21A2 is bound at the substrate entrance. The average crystallographic temperature factors of the proximal and distal 17OHP molecules in CYP21A2 are 64.8 and 72.5 Å^3 compared with 56.4 Å^3 for heme in the CYP21A2 structure, further indicating that each 17OHP substrate molecule in the four CYP21A2 structures occupies a slightly different position (Fig. 3).

The proximal substrate binding pocket is defined by several hydrophobic residues over the heme. The residues within 4 Å around the proximal 17OHP create a functional catalytic pocket. At the end of carbon C21 of 17OHP, Thr-294 in the central I helix is highly conserved in the majority of P450s and may be involved in stabilizing the dioxygen complex or assist in proton transfer (34). Val-358 and Leu-362, in the K-β4 loop, provide hydrophobic environments and van der Waals interactions. There are two hydrophobic residues directed toward the β face of 17OHP, Leu-110 in the B′-C loop and Trp-200 in the kink between the F and F′ helices. These two residues build a hydrophobic wall to avoid movement of solvent into the active site. At the 17OHP A-ring end, Arg-232 anchors the 3-keto oxygen through a hydrogen bond, as described earlier. At the bottom of 17OHP, Ser-109 (in the B′-C loop) and Asp-286 (in the I helix) lift the substrate to help Arg-232 hold it in the active site. At the top of 17OHP, the side chains of Leu-196 and Met-197 stretch like two wings along the F helix to fill gaps between the F/G helices and the F/β6, which may also provide hydrophobic protection against solvent. The volume of the proximal binding pocket is estimated to be about 600 Å^3. Altogether, these interactions between substrate and the active site residues dictate the orientation and location of the substrate toward the G helix and put C21 in a proper position in the reaction center.

The distal 17OHP binding region is composed of Leu-64, Gly-65, and Leu-66 in the β1/β2 loop, Ile-95 in the B-B′ loop, Gln-206 and Met-210 in the F′ helix, Leu-360 and Ala-361 in the K-β4 loop, and Cys-467 and Gly-468 in the β hairpin of β5/β6, all of which contact with the distal 17OHP molecule within 4 Å. These residues form a cavity in the substrate access channel (Fig. 5). It is worth noting that the A-ring of the distal 17OHP sits deep inside the channel, with the other end of the structure being partially exposed to solvent. In addition, the 3-keto oxygen forms hydrogen bonds with the carbonyl oxygen of Ala-361 at 3.3 Å and the carbonyl oxygen of Gly-468 at 3.6 Å. These interactions may indicate increased movement of the corresponding structural elements and also indicate that this cavity is triggered upon ligand binding to select the ligand on the distal surface of the protein. Furthermore, the weak hydrogen bonding contacts between the distal 17OHP and Ala-361/Gly-468 could be of importance for distal 17OHP binding and release.

Spectral Measurements—The structures provide evidence for the presence of two ligands in the active site (*i.e.* the substrate 17OHP). We carried out spectroscopic assays to provide additional evidence for the presence of multiple ligands.

Titration of CYP21A2 with 17OHP provided a plot that, upon visual inspection, showed very tight binding of a single molecule of substrate (to 2 μM), followed by a further increase in the heme spectral changes (Fig. 6). Fitting required very tight binding of a single molecule of the first molecule ($K_d \cong 50$ nM), with a second K_d of 0.7 μM. The fitting is not ideal in the absence of information about what the actual extinction coefficient is. In the case of progesterone (not shown), the break following binding of one ligand was not clear, and the results could be explained with a simple hyperbolic, unimolecular binding isotherm, corrected for the enzyme concentration ($K_d \cong 0.40 \pm 0.07$ μM), although a more complex relationship may exist.

Pre-steady-state binding also showed multiphasic behavior (Fig. 7). The spectral changes observed upon mixing of 20 μM (10-fold excess over CYP21A2) were relatively slow for the

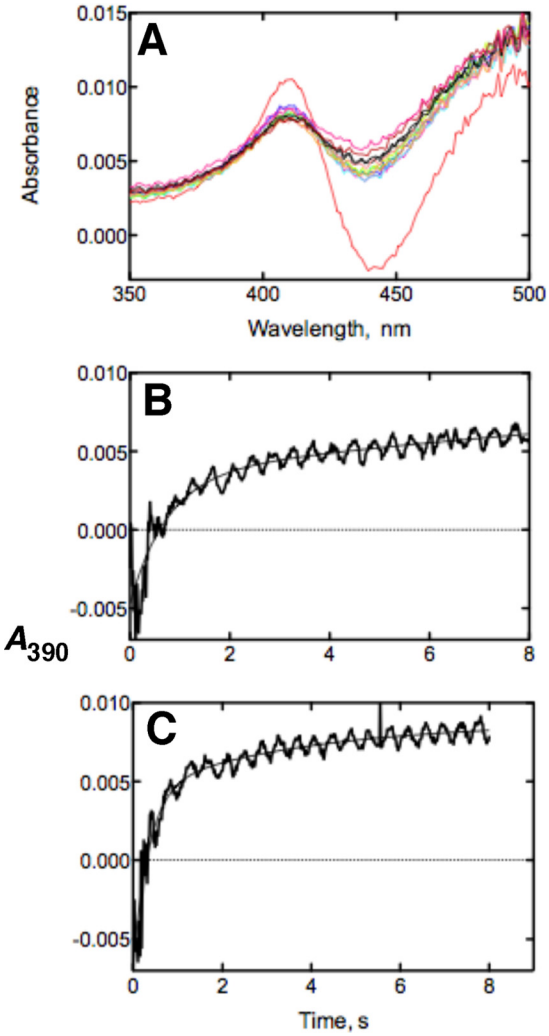

FIGURE 7. **Pre-steady-state binding of progesterone and 17OHP to CYP21A2.** Spectra were recorded in an OLIS-RSM 1000 instrument at 37 °C. One syringe contained 4 μM P450 21A2 in 50 mM potassium phosphate buffer (pH 7.4), 100 mM NaCl, 0.1 mM dithiothreitol, and 0.1 mM EDTA. The other syringe contained 40 μM progesterone or 17OHP in the same buffer. The components (equal volumes) were mixed, and spectra were acquired every 1 ms. Some of the early traces and the final trace (16 s) are shown in *A* (fully changed). ΔA_{390} data points were fit to biexponential plots using the manufacturer's software (GlobalWorks). *B*, progesterone binding. $k_1 = 1.8 \pm 0.7$ s^{-1}, $k_2 = 0.062 \pm 0.06$ s^{-1}. *C*, 17OHP binding. $k_1 = 2.5 \pm 0.3$ s^{-1}, $k_2 = 0.26 \pm 0.10$ s^{-1}.

rapid phase (1.8 and 2.5 s^{-1} for progesterone and 17OHP, respectively), followed by a slower phase with a rate 1 order of magnitude slower. The faster rate is considerably slower than expected for a diffusion-controlled process (*i.e.* 2 $s^{-1}/20$ μM $\cong$ 10^5 M^{-1} s^{-1}). The slow, multiphasic binding is consistent with the multisite binding of ligands to CYP21A2, although this observation alone cannot be considered a proof.

DISCUSSION

CYP21A2 is the cytochrome P450 with the largest number of naturally occurring mutants involved in steroidogenic hormone biosynthesis and is directly responsible for the largest number of cases of CAH (3, 5, 6). In general, the severity of the disease correlates well with the level of CYP21A2 enzymatic deficiency (35). The analysis of primary sequences of all mammalian CYP21A2 shows that >85% of the human CAH mutants occur in highly conserved residues. Thus, the conserved residues are expected to be crucial in maintaining the enzyme structure and function among species during the evolution. In addition, the locations of mutants are distributed throughout the structure, from the N-terminal region to the C-terminal loop, on all structural elements through loop regions, β sheets, and all α helices except the A and F′ helices. Helices I and G show the most hits among helical elements. About 55% of the mutants are located in loop structures, and many severe mutations are located in the meander region.

As noted above, the most intriguing result from this structure is that there are two bound molecules of 17OHP and therefore two distinct binding cavities located in the protein (Fig. 5). One is on the surface with the substrate access channel for the distal 17OHP and the other is buried into the heme pocket for the proximal 17OHP. There is a narrow U-shaped bottle neck channel linked between these two cavities. Both the structural and spectral/kinetic data may suggest that 17OHP could occupy two positions in the active site and that the distal 17OHP might be bifunctional in ensuring that substrate is bound to the distal binding site, subsequently dissociating and moving into the active site. Thus, it may help close the active site when the proximal substrate triggers the conformational changes.

Another interesting feature of CYP21A2 is that the geometries of the proximal 17OHP substrates in CYP21A2 are different from those in CYP11A1 (29). In CYP21A2, the A-ring end of the substrate is pointed toward the G helix. In contrast, the long side chain of the cholesterol in CYP11A1 is located above the heme in the reaction center, and the steroid backbone remains in the substrate access channel. In CYP11A1, the substrate access and product release probably share the same substrate access channel. However, CYP21A2 may have a different path for product exit because of the substrate orientation in the active site and the distal substrate blocking the channel. This raises the question of how the product would release from the CYP21A2 active site. An opening is formed by the N terminus of the I helix with the B′ and G helix. This leads to a channel that exits to the exterior of the protein surface. The Met-282, Val-285, and Asp-286 residues in the I helix, residues Ile-229, Arg-232, and Asp-233 in the G helix, and Val-101 and Gln-103 in the B′ helix line the channel. It is possible that this channel, although too narrow at certain points to let steroid products pass through, permits the passage of the product when the flexibility of the surrounding tertiary structure is taken into account.

Structural Basis of Human Variants—The sequence identity between bovine CYP21A2 and human enzyme is 79% (supplemental Fig. S1). However, 85% of the known mutations leading to CAH are identical. Moreover, all structural elements observed in bovine CYP21A2 are almost certainly present in the human structure. Therefore, the bovine structure is a close representation of the human structure.

To enhance understanding of the molecular mechanism of the disease, we analyzed the structural basis of 35 reported mutations (Table 2 and supplemental Fig. S3). In general, mutation of any one of these residues profoundly reduces the

enzyme activities. The mutants cause CAH through impairment of the CYP21A2 catalytic activity in multiple ways, such as interruption of substrate binding, breaking the proton relay system, inhibiting NADPH-P450 reductase interaction, affecting heme ligation, and reducing protein structure solubility, stability for substrate oxidation, and product release. All of these key functional residues are located in different secondary structural elements and generally cannot be deduced from homology modeling. Examples include the following.

Substrate Access—Gly-65 is located in the $\beta1/\beta2$ loop and is associated with the distal 17OHP (Fig. 8*A*). In a van der Waals model, the backbone carbon from Gly-65 is the only possible amino acid to fit the narrow substrate access opening. The long side chain of the variant G65E may block the substrate.

Substrate Binding—The α face of the proximal 17OHP is directed toward the I helix, and the 17α hydroxyl points into Gly-290 and Gly-291 located in the middle of the I helix so that a helical kink is created. Thus, human variants G291C, G291S, and G292D might have altered substrate binding in the active site in such a way as to eliminate activity. In addition, Tyr-98 is located in the B′ helix, and its aromatic side chain points to the active site. Tyr-98 is about 3.8 Å away from the side chain of Trp-200, which is involved in the proximal binding site. Tyr-98 may play a role in helping to close the active site and assist Trp-200 to inhibit movement of the solvent molecule into the heme pocket. Therefore, it is not surprising that Tyr-98 mutated to hydrophilic residues decreased the activity significantly (36).

Proton Transfer—Thr-294, in the I helix, is a highly conserved residue found in most P450s. The mutant T294N probably disrupts substrate binding because the hydroxyl group in Thr-294 is only 2.4 Å away from the C21 methyl group of the proximal 17OHP. Also, the asparagine might break the proton transfer path during the catalytic cycle (34).

Protein Solubility—Gln-227 is located at the third turn of the G helix. This residue is identified as a surface residue, and its side chain is exposed to solvent. In the structure, two water molecules (WAT90 and WAT98) could be nearby. This suggests that Gln-227 might change the protein hydrophilicity if changed to a nonpolar residue and lose its function as a structural stabilizer in CYP21A2.

Heme Binding—a common feature of all P450s is that the P450 folding and activity requires heme as prosthetic group. Several residues in CYP21A2 participate in heme binding. The heme group makes ionic and hydrogen bonding interactions (via its propionate moieties) with side chains of Arg-92, Arg-425, His-364, Trp-117, and Ser-109. The mutation R425H is likely to affect the heme ligation with the protein. In addition, both Ile-108 and Ala-361 are directed toward the heme at a distance 3.6 Å. The bulky side chain mutants for I108R and A361V may sterically clash with the heme, thus pushing it in the

TABLE 2
Proposed structural basis of disease-causing mutants of CAH

Human	Bovine	Assigned structural basis	Location
P30Q	P31Q	Stability	N-terminal loop
K54X	K55X	Stability	AB loop
G64E	G65E	Substrate	B1β2 loop
K74X	K75X	Reductase binding	B helix
G90V	G91V	Stability	BB′ loop
Y97X	Y98X	Solubility	B′ helix
L107R	I108R	Heme	B′C loop
V139E	V140E	Stability	D helix
L142P	L143P	Stability	D helix
L167P	L168P	Stability	E helix
Q228X	Q227X	Solubility	G helix
L261P	L260P	Stability	H
Q262X	Q261X	Stability	HI loop
G291C	G290C	Substrate	I
G291S	G290S	Substrate	I
G292D	G291D	Substrate	I
T295N	T294N	Proton transfer	I
W302R	W301R	Stability	I
R316X	R315X	Stability	J
L353R	L352R	Stability	K
R354C	R353C	E*XX*R	Kβ4 loop
R354H	R353H	E*XX*R	Kβ4 loop
R356P	R355P	Stability	Kβ4 loop
R356W	R355W	Stability	Kβ4 loop
A362V	A361V	Heme	Kβ4 loop
G375S	G374S	Stability	B3β4 loop
Y376X	Y375X	Stability	B3β4 loop
E380D	E379D	Stability	B3β4 loop
F404S	F403S	Stability	KL loop
W405X	R404X	Stability	KL loop
R408C	R407C	Stability	KL loop
R426H	R425H	Heme	KL loop
L446P	L445P	Stability	L helix
T450P	T449P	Stability	Lβ5 loop
Q481P, P482S	Q481P, P482S	Stability	C terminus
R483W	R483W	Stability	C terminus

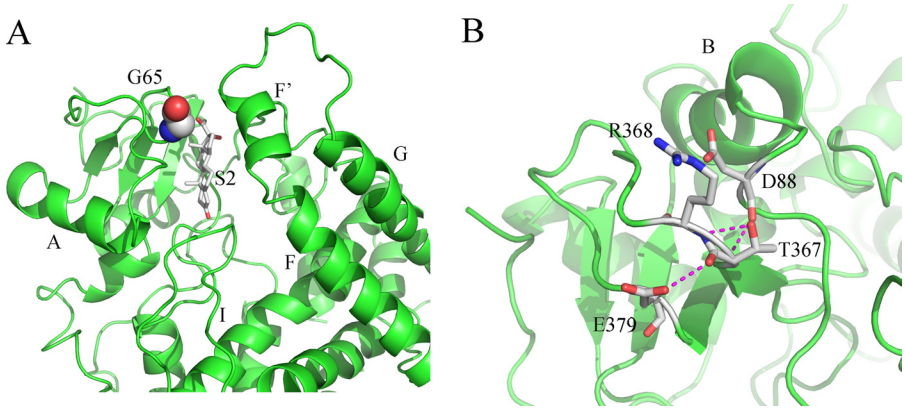

FIGURE 8. **Detailed local structural features of CYP21A2.** *A*, Gly-65 (in a van der Waals surface model) is located at the β-hairpin turn and is less than 4 Å from the distal substrate. It serves as a gating residue at the mouth of the substrate access channel; *B*, Glu-379 is directed toward the surface of the protein and at the loop between β1-3 and β1-4. The carbonyl group of Glu-379 can form a hydrogen bond with the oxygen of Thr-367, thus locking the two β sheets in the structure. Thr-367 makes an additional hydrogen bond with Asp-88, which is in the loop near the B helix. These hydrogen bond interactions play an important role in maintaining the structural fold. *Dotted lines* show the presumed hydrogen bonding network.

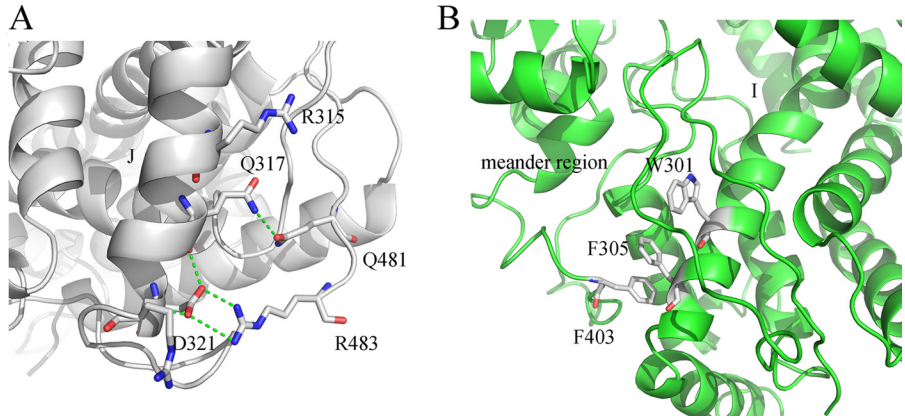

FIGURE 9. **The continuous hydrogen bonding network in the engineered CYP21A2 complexes.** *A*, Arg-483 and Gln-481 lie near the C-terminal end of the protein. The side chains of both Arg-483 and Gln-481 form hydrogen bonds with Asp-321 and Gln-317 in the J helix; *B*, the side chains of Trp-301, Phe-305, and Phe-403 form π-electron stacking interactions, thus linking the meander region and the C terminus of the I helix and stabilizing the structure.

opposite direction so that heme may not bind to the protein properly or not at all.

EXXR Structural Motif—The E*XX*R motif is highly conserved in essentially all P450 sequences (15) and is located in the K helix. The Glu and Arg and residues from the meander region can form a set of salt bridge/hydrogen bonding interactions that participate in the formation of the tertiary structure. There is evidence that suggests that E*XX*R is linked somehow to heme association with the P450 polypeptide (30, 37). In CYP21A2, Glu-350 and Arg-353 of the E*XX*R motif show standard ion pair interaction and also make hydrogen bonding interactions with residues Pro-400, Glu-402, Arg-404, Thr-347, and His-391 from the meander region. Substitution of Arg-353 to either histidine or cysteine in this position could disrupt the naturally occurring interactions with Glu-350, Pro-400, and His-391, essential for maintaining the folded structure.

Structural Stability—Some residues can extend the hydrogen bonding network or other molecular interactions between secondary structural elements. These residues, like a bridge, play important roles in properly integrating the secondary structural elements to stabilize the scaffold of the protein. The side chain of Glu-379 is directed toward the surface of the protein at the β4 loop (Fig. 8*B*). The carboxylic acid of Glu-379 can form a hydrogen bond with the carbonyl oxygen of Thr-367 located at the β3 loop, which locks the β3 and β4 sheets. Thr-367 extends hydrogen bonding interaction with Asp-88 at the BB′ loop via its backbone amide nitrogen. Thus, the three loops lie together via Glu-379, Thr-367, and Asp-88. The side chain of Glu-379 mutated to aspartic acid has one less carbon so that this mutation could break the interaction with Thr-367 to interrupt the β3, β4, and BB′ loop structure. Another example is that both Arg-483 and Glu-481 lie in β6 at the C terminus of the protein. The side chain Arg-483 can make a hydrogen bond with Asp-321 in the J helix (Fig. 9*A*). Gln-481 is able to make hydrogen bond connections with Gln-317 in the J helix and Gln-446 in the Lβ6 loop. Arg-315 in the J helix can connect with Asp-406 in the meander region through a hydrogen bond. These hydrogen bond networks may connect the C terminus, J helix, and meander region to maintain the structural elements in the correct positions. Any mutation on these residues probably results in the interruption of the networks. Thus, the human mutants R483W and Q481P/P482S lead to CAH. A third example of an interaction that may affect protein stability concerns the two aromatic rings of Trp-301 and Phe-305 from the C-terminal end of the I helix, which form π-electron stacking interactions with the side chain of Phe-403 in the meander region (these side chains all lie within 5 Å from each other; Fig. 9*B*). This structural feature stabilizes the meander region and the I helix. The stacking interactions require all three aromatic side chains. Replacement of any one of these amino acids by a non-aromatic residue will probably interrupt these interactions. This is the case for mutants W301R and F403S, both of which are clinically associated with CAH (38). Based on multiple sequence alignments, Trp-302 and Phe-403 are strictly conserved in all CYP21A2 sequences. Phe-305 exists in all mammals except in swine, where tyrosine is present, a residue that also features an aromatic side chain that may play an important role in bridging Trp-301 and Phe-402. It is interesting that aromatic residues at 301 and 402 in CYP21A2 can also be found at the corresponding residue in some other P450 enzymes, such as CYP2C5 (Tyr-305 and Phe-404), CYP11A1 (Trp-298 and Phe-396), and CYP19A1 (Phe-317 and Phe-413). What is not known, however, is whether non-aromatic substitution of these corresponding residues in other P450s would significantly reduce the catalytic activities and therefore might play similar roles as in CYP21A2.

NADPH-P450 Reductase Binding—Electron transfer through redox proteins is essential for P450 activity. It is believed that basic residues on the proximal face of P450s interact with acidic residues on the surface of the redox protein (39). Mutation of a cluster of basic residues on the proximal surface of CYP21A2 results in CAH. The basic residues consist of Arg-338, Arg-340, Lys-74, Arg-434, Arg-407, and Arg-368 and may be involved in a redox protein interaction according to the P450BM3 structure (40). Perhaps mutations of these residues can cause CAH by an inability to interact correctly with the redox partner. In summary, the crystal structure of CYP21A2 not only offers valuable information about CAH-associated residues in CYP21A2 and the etiology of CAH but also offers an enhanced understanding of the detailed structure/function relationships of P450s.

Acknowledgments—We thank Dr. Martin Egli for reading the manuscript and the personnel at the SER-CAT 22-BM and LS-CAT beamlines at APS/Argonne National Laboratory for technical assistance, M. V. Martin and L. M. Folkmann for preparation of NADPH-P450 reductase, and K. Trisler for help in the preparation of the manuscript.

REFERENCES

1. Kagawa, N., and Waterman, M. R. (1991) Evidence that an adrenal-specific nuclear protein regulates the cAMP responsiveness of the human CYP21B (P450C21) gene. *J. Biol. Chem.* **266,** 11199–11204
2. Kagawa, N., and Waterman, M. R. (1990) cAMP-dependent transcription of the human CYP21B (P-450C21) gene requires a cis-regulatory element distinct from the consensus cAMP-regulatory element. *J. Biol. Chem.* **265,** 11299–11305
3. White, P. C., and Speiser, P. W. (2000) Congenital adrenal hyperplasia due to 21-hydroxylase deficiency. *Endocr. Rev.* **21,** 245–291
4. Speiser, P. W., and White, P. C. (2003) Congenital adrenal hyperplasia. *N. Engl. J. Med.* **349,** 776–788
5. White, P. C., New, M. I., and Dupont, B. (1986) Structure of human steroid 21-hydroxylase genes. *Proc. Natl. Acad. Sci. U.S.A.* **83,** 5111–5115
6. White, P. C., Grossberger, D., Onufer, B. J., Chaplin, D. D., New, M. I., Dupont, B., and Strominger, J. L. (1985) Two genes encoding steroid 21-hydroxylase are located near the genes encoding the fourth component of complement in man. *Proc. Natl. Acad. Sci. U.S.A.* **82,** 1089–1093
7. Higashi, Y., Tanae, A., Inoue, H., Hiromasa, T., and Fujii-Kuriyama, Y. (1988) Aberrant splicing and missense mutations cause steroid 21-hydroxylase (P-450(C21)) deficiency in humans. Possible gene conversion products. *Proc. Natl. Acad. Sci. U.S.A.* **85,** 7486–7490
8. Krone, N., and Arlt, W. (2009) Genetics of congenital adrenal hyperplasia. *Best Pract. Res. Clin. Endocrinol. Metab.* **23,** 181–192
9. Robins, T., Carlsson, J., Sunnerhagen, M., Wedell, A., and Persson, B. (2006) Molecular model of human CYP21 based on mammalian CYP2C5. Structural features correlate with clinical severity of mutations causing congenital adrenal hyperplasia. *Mol. Endocrinol.* **20,** 2946–2964
10. Mornet, E., and Gibrat, J. F. (2000) A 3D model of human P450c21. Study of the putative effects of steroid 21-hydroxylase gene mutations. *Hum. Genet.* **106,** 330–339
11. Dauber, A., Kellogg, M., and Majzoub, J. A. (2010) Monitoring of therapy in congenital adrenal hyperplasia. *Clin. Chem.* **56,** 1245–1251
12. Concolino, P., Mello, E., Zuppi, C., and Capoluongo, E. (2010) Molecular diagnosis of congenital adrenal hyperplasia due to 21-hydroxylase deficiency. An update of new CYP21A2 mutations. *Clin. Chem. Lab. Med.* **48,** 1057–1062
13. Shaw, A. M. (2010) 21-hydroxylase deficiency congenital adrenal hyperplasia. *Neonatal Netw.* **29,** 191–196
14. Wedell, A. (2011) Molecular genetics of 21-hydroxylase deficiency. *Endocr. Dev.* **20,** 80–87
15. Rupasinghe, S., Schuler, M. A., Kagawa, N., Yuan, H., Lei, L., Zhao, B., Kelly, S. L., Waterman, M. R., and Lamb, D. C. (2006) The cytochrome P450 gene family CYP157 does not contain EXXR in the K-helix reducing the absolute conserved P450 residues to a single cysteine. *FEBS Lett.* **580,** 6338–6342
16. Arase, M., Waterman, M. R., and Kagawa, N. (2006) Purification and characterization of bovine steroid 21-hydroxylase (P450c21) efficiently expressed in *Escherichia coli*. *Biochem. Biophys. Res. Commun.* **344,** 400–405
17. Shen, A. L., Porter, T. D., Wilson, T. E., and Kasper, C. B. (1989) Structural analysis of the FMN binding domain of NADPH-cytochrome P-450 oxidoreductase by site-directed mutagenesis. *J. Biol. Chem.* **264,** 7584–7589
18. Hanna, I. H., Reed, J. R., Guengerich, F. P., and Hollenberg, P. F. (2000) Expression of human cytochrome P450 2B6 in *Escherichia coli*. Characterization of catalytic activity and expression levels in human liver. *Arch. Biochem. Biophys.* **376,** 206–216
19. Otwinowski, Z., Borek, D., Majewski, W., and Minor, W. (2003) Multiparametric scaling of diffraction intensities. *Acta Crystallogr. A* **59,** 228–234
20. Storoni, L. C., McCoy, A. J., and Read, R. J. (2004) Likelihood-enhanced fast rotation functions. *Acta Crystallogr. D Biol. Crystallogr.* **60,** 432–438
21. Emsley, P., Lohkamp, B., Scott, W. G., and Cowtan, K. (2010) Features and development of Coot. *Acta Crystallogr. D Biol. Crystallogr.* **66,** 486–501
22. Brünger, A. T., Adams, P. D., Clore, G. M., DeLano, W. L., Gros, P., Grosse-Kunstleve, R. W., Jiang, J. S., Kuszewski, J., Nilges, M., Pannu, N. S., Read, R. J., Rice, L. M., Simonson, T., and Warren, G. L. (1998) Crystallography & NMR system. A new software suite for macromolecular structure determination. *Acta Crystallogr. D. Biol. Crystallogr.* **54,** 905–921
23. Schüttelkopf, A. W., and van Aalten, D. M. (2004) PRODRG. A tool for high-throughput crystallography of protein-ligand complexes. *Acta Crystallogr. D. Biol. Crystallogr.* **60,** 1355–1363
24. Yeates, T. O. (1997) Detecting and overcoming crystal twinning. *Methods Enzymol.* **276,** 344–358
25. DeLano, W. L. (2010) *The PyMOL Molecular Graphics System*, version 1.2r3pre, Schrödinger, LLC, New York
26. Derewenda, Z. S. (2004) The use of recombinant methods and molecular engineering in protein crystallization. *Methods* **34,** 354–363
27. Ghosh, D., Griswold, J., Erman, M., and Pangborn, W. (2010) X-ray structure of human aromatase reveals an androgen-specific active site. *J. Steroid Biochem. Mol. Biol.* **118,** 197–202
28. Annalora, A. J., Goodin, D. B., Hong, W. X., Zhang, Q., Johnson, E. F., and Stout, C. D. (2010) Crystal structure of CYP24A1, a mitochondrial cytochrome P450 involved in vitamin D metabolism. *J. Mol. Biol.* **396,** 441–451
29. Mast, N., Annalora, A. J., Lodowski, D. T., Palczewski, K., Stout, C. D., and Pikuleva, I. A. (2011) Structural basis for three-step sequential catalysis by the cholesterol side chain cleavage enzyme CYP11A1. *J. Biol. Chem.* **286,** 5607–5613
30. Hasemann, C. A., Kurumbail, R. G., Boddupalli, S. S., Peterson, J. A., and Deisenhofer, J. (1995) Structure and function of cytochromes P450. A comparative analysis of three crystal structures. *Structure* **3,** 41–62
31. Strushkevich, N., Usanov, S. A., and Park, H. W. (2010) Structural basis of human CYP51 inhibition by antifungal azoles. *J. Mol. Biol.* **397,** 1067–1078
32. Zhao, B., Guengerich, F. P., Voehler, M., and Waterman, M. R. (2005) Role of active site water molecules and substrate hydroxyl groups in oxygen activation by cytochrome P450 158A2. A new mechanism of proton transfer. *J. Biol. Chem.* **280,** 42188–42197
33. Nagano, S., Cupp-Vickery, J. R., and Poulos, T. L. (2005) Crystal structures of the ferrous dioxygen complex of wild-type cytochrome P450eryF and its mutants, A245S and A245T. Investigation of the proton transfer system in P450eryF. *J. Biol. Chem.* **280,** 22102–22107
34. Nagano, S., and Poulos, T. L. (2005) Crystallographic study on the dioxygen complex of wild-type and mutant cytochrome P450cam. Implications for the dioxygen activation mechanism. *J. Biol. Chem.* **280,** 31659–31663
35. Jääskeläinen, J., Levo, A., Voutilainen, R., and Partanen, J. (1997) Population-wide evaluation of disease manifestation in relation to molecular genotype in steroid 21-hydroxylase (CYP21) deficiency. Good correlation in a well defined population. *J. Clin. Endocrinol. Metab.* **82,** 3293–3297
36. Krone, N., Roscher, A. A., Schwarz, H. P., and Braun, A. (1998) Comprehensive analytical strategy for mutation screening in 21-hydroxylase deficiency. *Clin. Chem.* **44,** 2075–2082
37. Hatae, T., Hara, S., Yokoyama, C., Yabuki, T., Inoue, H., Ullrich, V., and Tanabe, T. (1996) Site-directed mutagenesis of human prostacyclin synthase. Alteration of Cys-441 of the Cys-pocket and Glu-347 and Arg-350 of the E*XX*R motif. *FEBS Lett.* **389,** 268–272
38. Bleicken, C., Loidi, L., Dhir, V., Parajes, S., Quinteiro, C., Dominguez, F., Grötzinger, J., Sippell, W. G., Riepe, F. G., Arlt, W., and Krone, N. (2009) Functional characterization of three CYP21A2 sequence variants (p.A265V, p.W302S, and p.D322G) employing a yeast co-expression system. *Hum. Mutat.* **30,** E443–E450
39. Hlavica, P., Schulze, J., and Lewis, D. F. (2003) Functional interaction of cytochrome P450 with its redox partners. A critical assessment and update of the topology of predicted contact regions. *J. Inorg. Biochem.* **96,** 279–297
40. Sevrioukova, I. F., Li, H., Zhang, H., Peterson, J. A., and Poulos, T. L. (1999) Structure of a cytochrome P450-redox partner electron-transfer complex. *Proc. Natl. Acad. Sci. U.S.A.* **96,** 1863–1868